ACS APPLIED MATERIALS & INTERFACES

Research Article

www.acsami.org

# Chelating Agent-Free, Vapor-Assisted Crystallization Method to Synthesize Hierarchical Microporous/Mesoporous MIL-125 (Ti)

Nicholas D. McNamara and Jason C. Hicks*

Department of Chemical and Biomolecular Engineering, University of Notre Dame, 182 Fitzpatrick Hall, Notre Dame, Indiana 46556, United States

Supporting Information

**ABSTRACT:** Titanium-based microporous heterogeneous catalysts are widely studied but are often limited by the accessibility of reactants to active sites. Metal−organic frameworks (MOFs), such as MIL-125 (Ti), exhibit enhanced surface areas due to their high intrinsic microporosity, but the pore diameters of most microporous MOFs are often too small to allow for the diffusion of larger reactants (>7 Å) relevant to petroleum and biomass upgrading. In this work, hierarchical microporous MIL-125 exhibiting significantly enhanced interparticle mesoporosity was synthesized using a chelating-free, vapor-assisted crystallization method. The resulting hierarchical MOF was examined as an active catalyst for the oxidation of dibenzothiophene (DBT) with *tert*-butyl hydroperoxide and outperformed the solely microporous analogue. This was attributed to greater access of the substrate to surface active sites, as the pores in the microporous analogues were of inadequate size to accommodate DBT. Moreover, thiophene adsorption studies suggested the mesoporous MOF contained larger amounts of unsaturated metal sites that could enhance the observed catalytic activity.

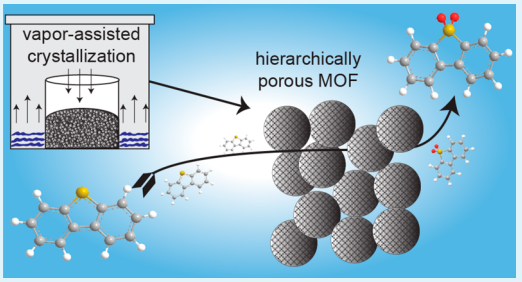


**KEYWORDS:** *oxidative desulfurization, metal−organic framework, dry gel conversion, oxidation, sulfur removal, heterogeneous catalysis*

## 1. INTRODUCTION

Titanium-based solid materials have been widely studied as heterogeneous catalysts due to their semiconductor properties in photocatalysis reactions and their proclivity to activate peroxides for oxidation reactions.[1,2] Typically, desired features of heterogeneous catalysts include high surface areas and high accessibility to active sites for enhanced catalytic efficiency. Ti-containing metal−organic frameworks (MOFs), namely, MIL-125 and its amine-functionalized analogue ($NH_2$-MIL-125), have shown great promise and versatility as heterogeneous catalysts in both photocatalytic and oxidation reactions.[3−11] These Ti-based MOFs were demonstrated to be active photocatalysts for a number of reactions including $CO_2$ reduction,[4] nitrobenzene reduction,[5] and hydrogen production from an aqueous medium.[6] Moreover, both MIL-125 and $NH_2$-MIL-125 have been reported as stable and active oxidation catalysts for various organic substrates.[7−9]

While these Ti-based MOFs have shown potential as heterogeneous catalysts, their practical applicability is limited due to their intrinsically microporous structures, which exclude larger molecules from diffusing into the pores and thus eliminate access to many potential active sites. As a specific example, and the highlight of this manuscript, MIL-125 has been reported to catalyze the oxidation of sulfur-containing dibenzothiophene (DBT, molecular dimensions of 8 × 12.2 Å[8]). From powder X-ray diffraction (XRD) experiments, the MIL-125 structure was retained and stable throughout the reaction, but it displayed a much lower activity compared to materials with larger pores due to its inadequate pore size (∼5−7 Å windows[3]), which prohibited the substrate from diffusing into the MOF structure.[8,9]

The versatility of MOFs does allow for the expansion of pore size via the use of longer ligands, and indeed some groups have been successful in the synthesis of larger pore sizes (up to ∼100 Å) for many transition metal MOFs.[12−14] Frequently, however, these attempts lead to more fragile frameworks that collapse upon desolvation or result in large void spaces that render the MOFs susceptible to self-interpenetration, which diminishes porosity.[14,15] Admittedly, even our own attempts at expanding the pore size of Ti-based MOFs by introducing extended ligands have been met with much resistance.

As an alternative to expansion of intrinsic pore sizes, the incorporation of hierarchical pore systems in MOFs via the addition of mesopores (or even macropores) can alleviate mass transport limitations.[16−24] Adding larger mesopores to MOF structures can allow bulkier substrates access to additional active sites and enhance diffusion rates by cutting diffusion path lengths leading to increased catalytic activity.[24] The addition of mesoporosity to MOFs has generally been accomplished through the use of soft template methods.[16−22] In these methods, either ionic surfactants or block copolymers are used to form micelles in precursor solutions around which the MOFs

Received: December 12, 2014
Accepted: February 19, 2015
Published: February 19, 2015





DOI: 10.1021/am508799d
ACS Appl. Mater. Interfaces 2015, 7, 5338−5346

can crystallize. The soft template is removed via common methods such as washing or calcination, leaving meso-sized voids in the crystalline MOF materials. When using soft templates, chelating agents or functionalized precursor/template molecules are usually necessary to bind the precursor metal ions to the template in order to avoid phase separation.[19,25] These chelating agents are frequently incorporated into the final MOF structure and cannot be removed without negatively impacting physical properties.[19,25,26] Furthermore, studies to determine the correct chemical functionality and amount of chelating agent are generally required to obtain a cooperative template effect resulting in mesoporosity. Alternatively, in the case of zeolite syntheses, aggregates of nanosized microporous zeolite particles displaying interparticle mesoporosity have been attained via the use of surfactants during dry gel conversion.[27−29] In this method, it has been suggested that surfactant molecules can act as capping agents for the precursors and create a confined environment that limits particle growth resulting in mesoporous aggregates of microporous zeolite crystallites. While no literature currently documents this type of surfactant/dry gel synthesis of micro/mesoporous MOFs, multiple studies feature the use of surfactants as capping agents to control particle growth and morphology of MOFs in solvothermal syntheses.[30−34]

Herein, we report the synthesis of hierarchically microporous/mesoporous (Ti) MIL-125 using a method that precludes the need for a chelating agent. This is, to the best of our knowledge, the first example of a synthetic route yielding MIL-125 exhibiting mesoporosity. In our vapor-assisted crystallization method (VAC, Figure 1), we aimed to bypass

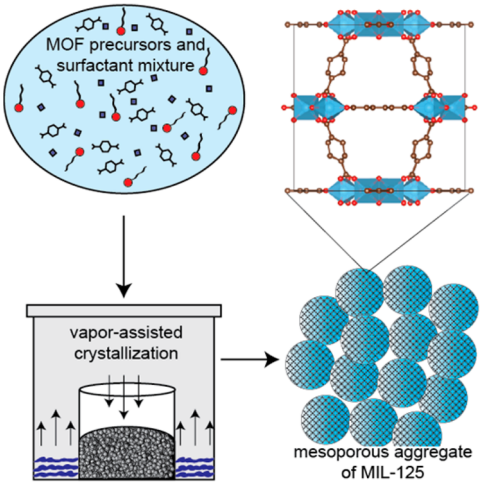


**Figure 1.** Cartoon representation of the formation of hierarchically microporous/mesoporous MIL-125 via the VAC method.

the need for a chelating agent wherein an interaction between the MOF precursors and the surfactant was forced by immobilizing the precursors in a dry gel creating a confined environment for MOF crystallization to occur.

## 2. EXPERIMENTAL SECTION

**2.1. Materials.** The following materials were commercially available and used as received: 1,4-benzenedicarboxylic acid (BDC, Sigma-Aldrich), titanium isopropoxide ($Ti(O\text{-}iPr)_4$, Acros Organics), decane (Alfa Aesar), dodecane (Alfa Aesar), dibenzothiophene (DBT, Acros Organic), *tert*-butyl hydroperoxide (5.0−6.0 M in decane, TBHP, Sigma-Aldrich), cetyltrimethylammonium bromide (CTAB, Sigma-Aldrich). Methanol (MeOH, BDH) and *N*,*N*-dimethylformamide (DMF, EDM) were dried over 3 Å molecular sieves and stored in a nitrogen glovebox prior to use.

**2.2. Solvothermal Synthesis of Microporous MIL-125.** Microporous MIL-125 synthesized solvothermally was prepared using a modified procedure reported by Dan-Hardi et al.[3] In a dry glovebox, 1.5 mmol of BDC was added to a solution of 4.25 g of dry DMF and 0.32 g of dry MeOH in a 44 mL teflon sleeve. A 0.35 mmol portion of $Ti(O\text{-}iPr)_4$ was then added to the solution and stirred for 5 min. The teflon sleeve containing the precursor solution was then sealed in a stainless steel reactor vessel, removed from the glovebox, and heated to 150 °C under autogenous pressure for 20 h. The resulting powder product was washed and centrifuged three times with DMF and three times with MeOH at a speed of 2000 rpm. The product was then dried overnight in a vacuum oven at 45 °C and calcined at 200 °C for 6 h.

**2.3. Vapor-Assisted Crystallization (VAC) Synthesis of Microporous MIL-125.** In a dry glovebox, 6.59 mmol of BDC was added to 2 mL MeOH in a 100 mL round-bottom flask. Approximately, 1.55 mmol of $Ti(O\text{-}iPr)_4$ was added to the solution and stirred for 5 min. The MeOH was then removed under vacuum at room temperature. A 0.349 g (containing 0.35 mmol of $Ti(O\text{-}iPr)_4$) aliquot of the resulting precursor powder was then transferred to a perfluoroalkoxy (PFA) cup. The PFA cup was then placed in a 44 mL Teflon sleeve, which contained a solution of 4.25 g DMF and 0.32 g MeOH. The teflon sleeve was sealed in a stainless steel reactor vessel, removed from the dry glovebox, and heated to 150 °C under autogenous pressure for 20 h. The resulting powder product was washed and centrifuged three times with DMF and three times with MeOH at a speed of 2000 rpm. The product was then dried overnight in a vacuum oven at 45 °C and calcined at 200 °C for 6 h.

**2.4. Vapor-Assisted Crystallization (VAC) Synthesis of Mesoporous MIL-125.** In a dry glovebox, 6.59 mmol of BDC and varying amounts of CTAB were added to 2 mL MeOH in a 100 mL round-bottom flask. Approximately 1.55 mmol of $Ti(O\text{-}iPr)_4$ was added to the solution and stirred for 5 min. The MeOH was then removed under vacuum at room temperature. An aliquot (containing 0.35 mmol of $Ti(O\text{-}iPr)_4$) of the resulting precursor powder was then transferred to a PFA cup. The PFA cup was then placed in a 44 mL teflon sleeve which contained a solution of 4.25 g DMF and 0.32 g MeOH. The teflon sleeve was sealed in a stainless steel reactor vessel, removed from the dry glovebox, and heated to 150 °C under autogenous pressure for 20 h. The resulting powder product was washed and centrifuged three times with DMF and three times with MeOH at a speed of 2000 rpm. The product was then dried overnight in a vacuum oven at 45 °C and calcined at 200 °C for 6 h.

**2.5. Catalytic Oxidation of Dibenzothiophene.** A solution containing 21.9 g of decane (solvent), 0.5 g of dodecane (internal standard), and 0.35 mmol DBT (reactant) was prepared in a stirred 100 mL round-bottom flask and heated to 80 °C in an oil bath. The flask was purged with flowing nitrogen for 30 min while temperature was reached and then capped. An initial sample for gas chromatography (GC) analysis was taken and then the appropriate MIL-125 catalyst was added in the amount of 88 $\mu$mol Ti metal centers. Once the temperature was stabilized, TBHP in a molar ratio of 10:1 of TBHP/DBT was then added to the solution. The addition of the TBHP signified the start of the reaction as a blank experiment in which no TBHP was added showed no detectable conversion. Approximately 0.5 mL aliquots of reactant solution were taken at predetermined times and diluted with hexane before GC analysis. Samples were then analyzed using an Agilent Technologies model 7820A gas chromatograph system. The GC was equipped with a flame ionization detector (FID) and utilized a (5%-phenyl)-methylpolysiloxane column (30 m, 0.32 mm diameter). Helium flowing at a rate of 0.5 mL $min^{-1}$ was used as the carrier gas and the column temperature was initially held at 50 °C for 3 min before being heated to 280 °C at a ramp rate of 15 °C $min^{-1}$. The concentration of DBT in the sample solutions was quantified using dodecane as an internal standard.

For recycle studies, a decane solution containing a catalyst concentration of 7.7 $\mu mol_{Ti}$ $mL^{-1}$ and a DBT concentration of 58.7


DOI: 10.1021/am508799d
ACS Appl. Mater. Interfaces 2015, 7, 5338−5346

$\mu$mol mL$^{-1}$ was used for all initial and subsequent recycle reactions. After each reaction, the catalyst was recovered by filtration and washed with ~150 mL of DMF then ~150 mL of MeOH. The catalyst was then vacuum-dried overnight at 40 °C and analyzed for Ti content via TGA analysis.

**2.6. Heat of Adsorption Measurements on TGA.** The heat of adsorption for thiophene on the MIL-125 samples was measured using a Mettler-Toledo TGA/DSC STAR System. In a typical experiment, 10 mg of sample was heated from room temperature to 150 °C at a ramp rate of 10 °C min$^{-1}$ and held for 30 min to desorb any water or solvent species. Samples were then cooled to 90 °C at a ramp rate of −10 °C min$^{-1}$. At this point, nitrogen gas flowing at 20 mL/min was bubbled through thiophene (B.P. = 84 °C) and over the sample for adsorption. Both weight change of the sample and heat flow were measured as a function of time as thiophene adsorbed onto the sample. Heat of adsorption ($\Delta H_{ads}$) was calculated by assuming weight change ($\Delta$Wt) and heat flow (HF) at each discrete time interval ($\Delta t$) was solely due to thiophene adsorption using the following equation:

$$\Delta H_{ads} = \frac{HF \times \Delta t}{\Delta \mathrm{Wt}/MW_{thiophene}} = \frac{Q}{n_{thiophene}}$$

**2.7. Characterization.** X-ray diffraction (XRD) patterns of the metal−organic frameworks (MOFs) were collected using a Bruker D8 Advance Davinci diffractometer operated at 40 mA and 40 kV with monochromated Cu K$\alpha$ radiation. Patterns were collected using a scan speed of 0.75 s/step and a step size of 0.02° at a 2$\theta$ range of 5−55°. Surface area and pore volume analysis was performed using isotherms collected by $N_2$ adsorption and desorption at 77 K using a Quantachrome NOVA 2200e. Prior to analysis, all samples were dried overnight under dynamic vacuum of $10^{-5}$ Torr at 125 °C. Thermogravimetric analysis (TGA) was performed on a Mettler-Toledo TGA/DSC STAR System in order to determine the titanium wt % of the MIL-125 samples. Samples were heated at a rate of 10 °C min$^{-1}$ from room temperature to 650 °C in order to combust all organic material. Titanium wt % was then calculated by assuming all material remaining after combustion was solely composed of $TiO_2$. This method of Ti wt % analysis was confirmed by a concurrent study in which multiple MIL-125 samples were analyzed by inductively coupled plasma optical emission spectroscopy (ICP-OES). Scanning electron microscopy (SEM) images were taken using a FEI-Magellan 400 FESEM. The materials were deposited onto a piece of carbon tape and mounted to a microscope stud. A sputtered layer of 2.5 nm of Ir was then deposited on samples prior to analysis to counteract charging effects. Transmission electron microscopy (TEM) images were collected using a FEI Titan 80−300 transmission electron microscope operating at 300 keV. Samples for TEM were prepared by suspension in methanol followed by sonication for a few minutes and then dropped onto a copper grid with a holey carbon support. UV−vis data were acquired using an Ocean Optics DH-2000 UV−vis-NIR light source.

## 3. RESULTS AND DISCUSSION

While examples of MOFs produced via dry gel conversion syntheses have been documented, these methods have not been used to introduce mesoporosity.[35,36] Moreover, synthesis of Ti-based MIL-125 using a vapor-assisted method has not yet been reported. Therefore, temperature and solvent studies were first performed to optimize the synthesis of microporous MIL-125 using the VAC method, and the resulting materials were characterized by XRD and $N_2$ physisorption. Synthesis temperatures were varied from 113 to 175 °C (at 92% DMF by vol), and it was found from XRD results that a crystalline MOF was produced at all temperatures. However, MIL-125 synthesized below 150 °C still contained a significant amount of unreacted precursor materials as evidenced by diffractions in the XRD patterns (Figure S1, Supporting Information) originating from BDC (organic ligand). Figure 2 shows an

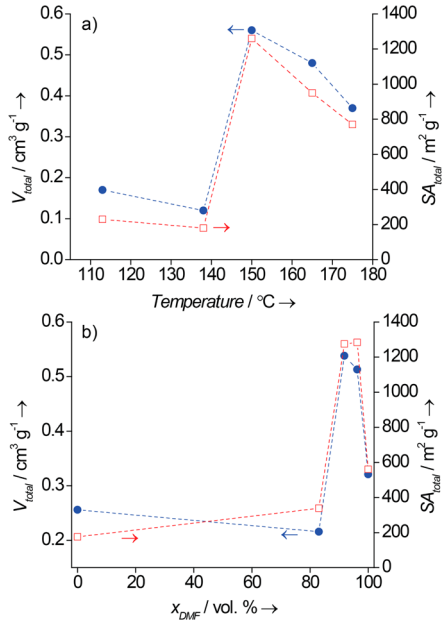


**Figure 2.** Effect of (a) synthesis temperature and (b) DMF vol % on MIL-125 textural properties in the VAC synthesis; (blue ●) total pore volume and (red □) total surface area calculated using the NLDFT method.

analysis of the textural properties as a function of synthesis temperature and reveals that pore volumes and surface areas of the materials were poor when synthesized at temperatures less than 150 °C as well. Furthermore, synthesis at 150 °C resulted in optimum textural properties, and an increase in temperature yielded diminished pore volumes and surface areas.

A solvent study was performed in which different volume percentages of DMF (with the balance being MeOH) were used in synthesis of MIL-125 using the VAC method. XRD patterns (Figure S2, Supporting Information) showed that syntheses in pure DMF down to 83.3% by volume DMF did produce the crystalline MIL-125 structure. The textural properties depicted in Figure 2, however, reached a maximum when 92% DMF by volume was used. It should be noted that synthesis was attempted in pure MeOH as well, and it was found that the MIL-125 structure was not evident in the XRD pattern and resulted in inferior textural properties. The optimum textural properties were produced by conducting the synthesis at 150 °C and 92% DMF by volume (balance being MeOH). $N_2$ physisorption data (Figures S3 and S4, Supporting Information) of the optimum VAC sample (denoted as VAC-micro-MIL-125) displayed a Type 1 isotherm indicative of a microporous material and was similar in shape and $N_2$ uptake to a solvothermally synthesized MIL-125 sample. Additionally, VAC-micro-MIL-125 displayed similar textural properties (Table 1) to solvothermally synthesized microporous MIL-125 (solv-micro-MIL-125). Furthermore, the XRD pattern of the VAC-micro-MIL-125 sample matched the calculated pattern from the original CIF (Figures S1 and S2, Supporting Information).[3]

Having demonstrated that the VAC method could produce crystalline MIL-125, we subsequently performed a CTAB concentration study in an attempt to construct a MOF displaying enhanced mesoporosity. The amount of CTAB added to the precursor solution was varied from slightly below the critical micelle concentration (CMC) for CTAB in 2 mL of


DOI: 10.1021/am508799d
ACS Appl. Mater. Interfaces 2015, 7, 5338−5346

**Table 1. Textural Properties, Kinetic Analysis Data, and Thiophene Adsorption Data for Microporous and Hierarchically Microporous/Mesoporous MOFs Synthesized via Solvothermal and VAC Methods**

| material[a] | $v_{total}$ ($cm^3\ g^{-1}$)[b] | $SA_{total}$ ($m^2\ g^{-1}$)[b] | $k_{app} \times 10^3$ ($min^{-1}$)[c] | $SA_{accessible}$ ($m^2\ g^{-1}$)[d] | $r''_0 \times 10^7$ ($mol_{DBT}\ min^{-1}\ m^2_{accessible}$)[e] | $\Delta H_{ads}$ ($kJ\ mol^{-1}$)[f] | thiophene capacity ($mol_{thio}\ mol_{Ti}$)[f] |
|---|---|---|---|---|---|---|---|
| solv-micro-MIL-125 | 0.54 | 1300 | 11.8 | 98 | 21.9 | −48.2 | 0.55 |
| VAC-micro-MIL-125 | 0.56 | 1260 | 11.6 | 91 | 22.0 | −47.6 | 0.53 |
| meso-MIL-125 | 0.91 | 975 | 22.9 | 190 | 22.0 | −49.9 | 0.65 |

[a]All material properties were determined by taking the average value for three or more samples. [b]Determined by nonlocal density functional theory analysis of $N_2$ adsorption/desorption isotherms. [c]Determined by fitting experimental data to a pseudo-first-order model. [d]Determined by t-plot method analysis of $N_2$ adsorption/desorption isotherms ($SA_{accessible} = SA_{meso} + SA_{external}$). [e]Initial reaction rate (after 30 min) normalized on surface area of catalyst ($r''_0$). [f]Heat of adsorption and thiophene capacity calculated using thiophene adsorption study on TGA (see the Experimental Section for details).

MeOH (volume of the precursor solution) up to a molar ratio 0.45 mol CTAB per mol of Ti. Representative $N_2$ adsorption−desorption isotherms and pore size distributions (calculated using the Barrett−Joyner−Halenda (BJH) analysis method on the $N_2$ desorption isotherm) are shown in Figure 3. The

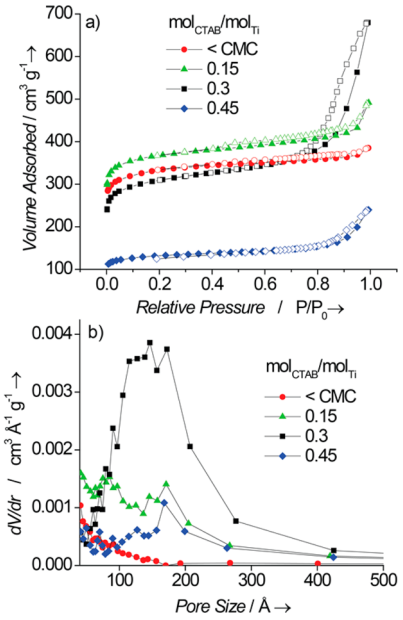


**Figure 3.** Effect of CTAB amount used in the VAC synthesis of MIL-125 on (a) $N_2$ adsorption−desorption isotherms and (b) mesopore size distribution (calculated using the BJH method on the desorption isotherm). The closed and open symbols in the $N_2$ isotherms represent adsorption and desorption portions, respectively.

material synthesized with less than the CMC amount of CTAB exhibited a Type I isotherm indicative of a solely microporous material. Moreover, the pore size distribution did not show any pores in the mesopore region. All three samples synthesized with CTAB > CMC displayed isotherms that were a mix between Type I, indicating micropores, and Type IV, indicating mesopores. The sample synthesized at CTAB/Ti molar ratio of 0.3, however, displayed a vastly larger $N_2$ uptake and more pronounced hysteresis in the high-pressure region, which suggested a greater mesoporosity. Additionally, all samples contained some mesopores in the range of ∼75−200 Å. Furthermore, the CTAB/Ti = 0.3 sample showed a more pronounced mesopore size distribution centered at ∼150 Å.

Textural properties for all samples are shown in Figure 4. When the amount of CTAB used was less than the CMC, no

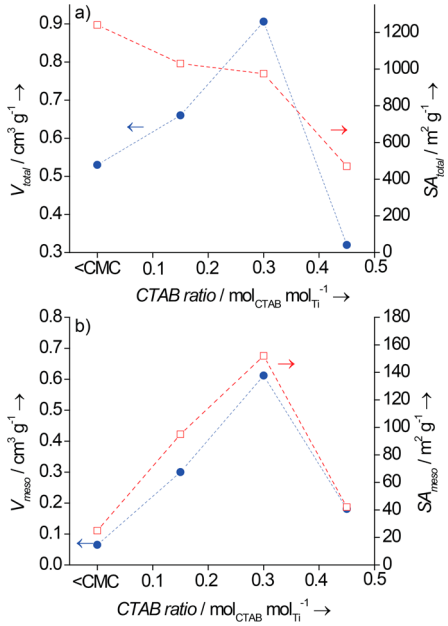


**Figure 4.** Effect of CTAB amount used in the VAC synthesis of MIL-125 on the (a) total pore properties (calculated using the NLDFT method) and (b) mesopore properties (calculated using the BJH method); (blue ●) total pore and mesopore volume and (red □) total and mesopore surface area.

mesoporosity was observed, and the resulting MOF's physical properties were similar to VAC-micro-MIL-125 without CTAB. As the CTAB/Ti molar ratio was increased past the CMC, the total surface area (calculated from $N_2$ physisorption isotherms using the nonlocal density functional theory (NLDFT)) continually decreased. This could be the result of a loss in crystallinity when higher amounts of CTAB are used, as Sakthivel et al. found similar results in their synthesis of mesoporous $\beta$-zeolites using a similar dry gel method.[29] They suggested an excess amount of surfactant present in the synthesis gel could lead to collapse and agglomeration during the drying and steaming processes resulting in an inhibition of crystallization. The total pore volume, however, increased as CTAB was increased, until it reached a maximum at 0.91 $cm^3\ g^{-1}$ when the molar ratio of CTAB/Ti = 0.3, which was ∼1.6× higher than the pore volume of VAC-micro-MIL-125 (0.56 $cm^3\ g^{-1}$). The mesopore volume and mesopore surface area also followed this upward trend, reaching a maximum at CTAB/Ti = 0.3 ($V_{meso}$ = 0.61 $cm^3\ g^{-1}$, $SA_{meso}$ = 150 $m^2\ g^{-1}$). Total pore volume, mesopore volume, and mesopore surface area then significantly decreased when the CTAB/Ti was increased to


DOI: 10.1021/am508799d
ACS Appl. Mater. Interfaces 2015, 7, 5338−5346

0.45 $mol_{CTAB}/mol_{Ti}$. From experiments with higher concentrations of CTAB (CTAB/Ti = 0.6), the CTAB appeared to disrupt MOF crystallization, as the crystalline MOF did not form during VAC synthesis. This is in agreement with results obtained by both Naik et al.[27] and Sakthivel et al.[29] for mesoporous zeolites synthesized with CTAB in a dry gel conversion method. Sakthivel, in particular, found that when relatively high amounts of CTAB were used, the resulting zeolite suffered from diminished textural properties and a further increase of the CTAB concentration completely suppressed zeolite crystallization.[29]

Further characterization of the optimum mesoporous sample (CTAB/Ti = 0.3, hereafter referred to as meso-MIL-125) was crystalline MIL-125 was evidenced by its diffraction pattern (Figure S5, Supporting Information). Moreover, no diffractions that could be assigned to BDC or CTAB were observed. SEM and TEM images are shown in Figure 5 (additional TEM images are shown in Figure S6, Supporting Information). SEM images revealed the meso-MIL-125 sample was mostly composed of large (>40 $\mu$m) agglomerations of small (<50 nm) nanoparticles, which created a sponge-like morphology wherein the interparticle mesopore voids could clearly be seen as the darker spots on the aggregated structure. TEM images further confirmed what was seen in the SEM images showing large agglomerations of small nanoparticles. Moreover, by focusing on a thin portion of the sample, the higher resolution in TEM enabled imaging of the individual mesopore voids (dashed circles) between nanoparticles. These mesopore voids were nonuniform and in the same size range as that calculated from $N_2$ physisorption data. To validate that this mesoporosity was permanent, the MOF was placed under mechanical stress. During the synthesis of meso-MIL-125, the as-synthesized powders were subjected to six cycles of centrifugation at 2000 rpm prior to characterization. These centrifugation cycles induced significant mechanical stress on the material, which indicated the mesoporosity was permanent, even upon the application of physical stress. To further test this conclusion, the meso-MIL-125 material was also subjected to sonication in methanol prior to both $N_2$ physisorption and TEM analysis and still exhibited similar textural properties (before sonication: $SA_{total}$ = 975 $m^2\ g^{-1}$, $V_{total}$ = 0.906 $cm^3\ g^{-1}$, $SA_{meso}$ = 152 $m^2\ g^{-1}$, and $V_{meso}$ = 0.612 $cm^3\ g^{-1}$ and after sonication: $SA_{total}$ = 1033 $m^2\ g^{-1}$, $V_{total}$ = 0.928 $cm^3\ g^{-1}$, $SA_{meso}$ = 169 $m^2\ g^{-1}$, and $V_{meso}$ = 0.650 $cm^3\ g^{-1}$). The slight increase in textural properties after sonication can be attributed to further washing of free organic molecules.

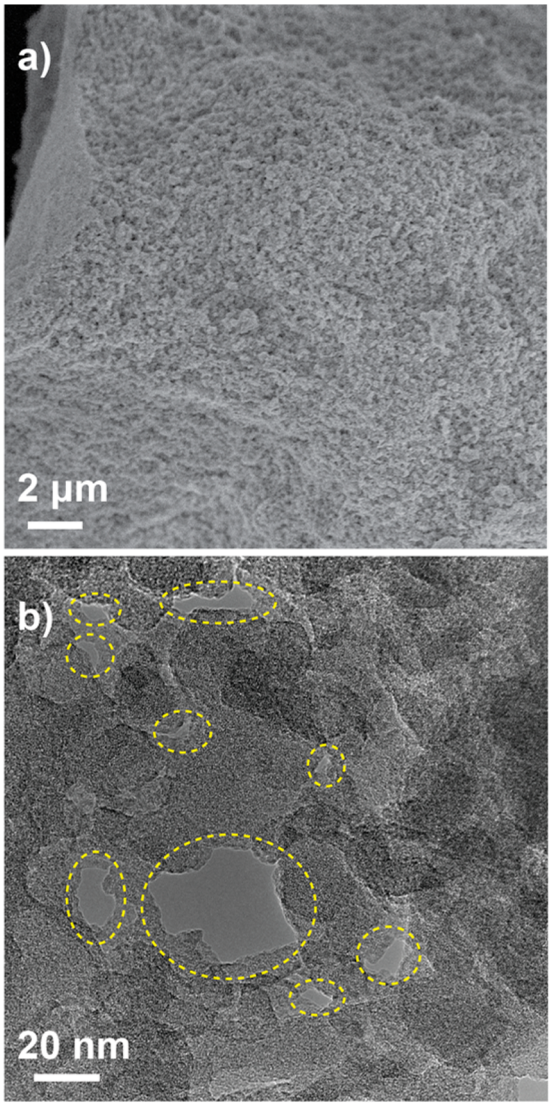


**Figure 5.** (a) SEM and (b) TEM images of the hierarchically porous meso-MIL-125. Dashed circles in the TEM image highlight the locations of mesopores.

TGA analysis (Figure S7, Supporting Information) in air revealed that meso-MIL-125 exhibited two major weight loss regions at the same temperatures as its microporous analogues, indicating that the addition of mesopores did not negatively impact the MOF's thermal stability. The first weight loss region occurred in the range of 25−200 °C and was attributed to the evacuation of guest molecules from the pores; the second weight loss region, which began at ∼300 °C, was due to the degradation of the MOF framework.[3] Ti wt % was calculated from TGA data (and confirmed by ICP-OES) by assuming the MOFs were completely combusted to yield $TiO_2$. Furthermore, it was determined that meso-MIL-125 generally contained ∼21−23% Ti by weight, which was similar to its microporous analogues. The actual Ti wt % was slightly lower than the theoretical value (at 24.5%), which could be attributed to the presence of guest molecules trapped in the pores of the MOF. UV−vis data were then used to investigate the possibility of $TiO_2$ domains present in the materials. MIL-125 has been shown to absorb UV light with an absorption edge of 350 nm[4], while that of $TiO_2$ is 400 nm.[37] The solvothermal, VAC, and meso-MIL-125 samples all displayed absorption edges at 350 nm in UV−vis spectroscopy (Figure S8, Supporting Information), indicating the lack of $TiO_2$ domains.

We then performed CTAB concentration studies in a solvothermal method in an attempt to add mesoporosity to MIL-125. As the CTAB amount was increased, only a minor increase in mesopore surface area (from 20 to 36 $m^2\ g^{-1}$) and volume (from 0.04 to 0.15 $cm^3\ g^{-1}$) was observed at CTAB/Ti = 0.6 (Figure S9, Supporting Information). Additionally, a plot of the differential volume as a function of pore size did not show any noticeable peaks, indicating a lack of uniform mesopores (Figure S10, Supporting Information). Furthermore, as CTAB was increased past CTAB/Ti = 0.6, both mesopore and total pore properties decreased, likely due to high concentrations of CTAB once again disrupting MOF formation. This was confirmed in an additional synthesis in which a high CTAB/Ti = 5 ratio was used and no MOF


DOI: 10.1021/am508799d
ACS Appl. Mater. Interfaces 2015, 7, 5338−5346

**Scheme 1. Schematic Representation of Mesoporous MIL-125 Formation**

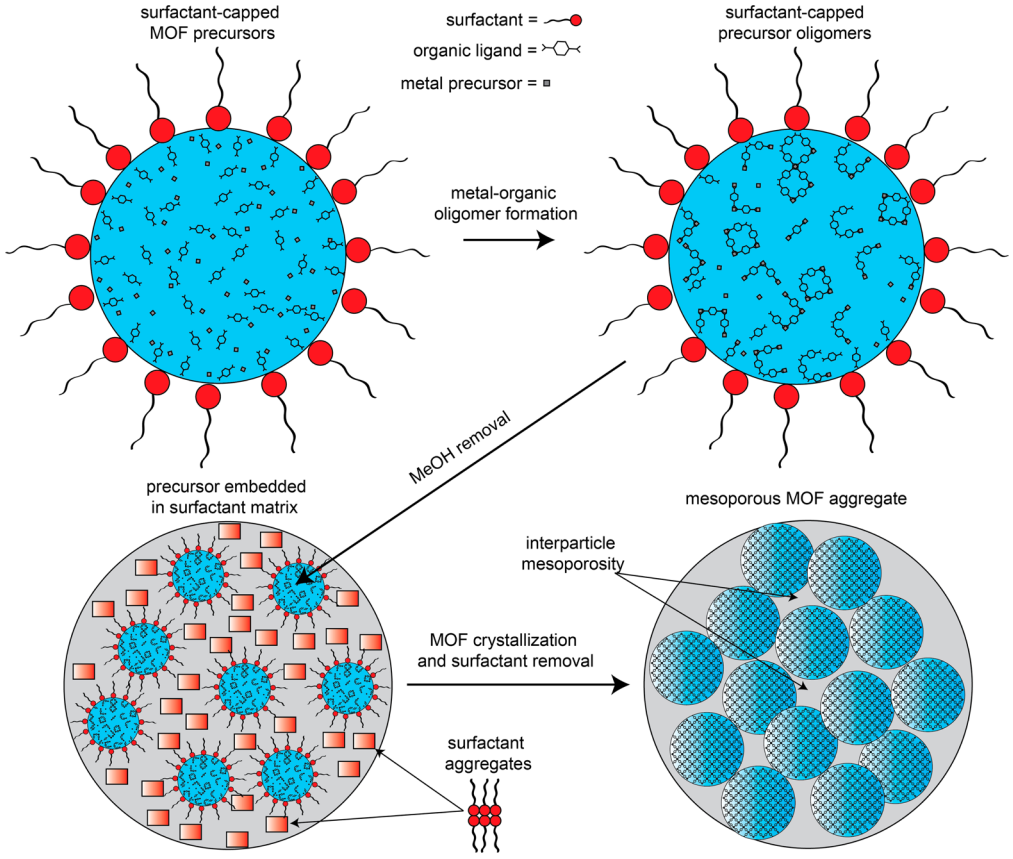


formation occurred. These results suggested that synthesis in the VAC method did not proceed through a simple solvothermal mechanism.

Experimental synthesis results in conjunction with a search of the relevant literature enabled us to propose a mechanism of MOF formation (Scheme 1). In the VAC method, a solid precursor powder is initially formed when the organic ligand (BDC) and the surfactant (CTAB) are mixed in a small amount of MeOH. Upon addition of $Ti(O\text{-}iPr)_4$, this solution undergoes a sudden and dramatic increase in solution viscosity, which indicates strong chemical interactions are taking place (Scheme S1, Supporting Information). Multiple interactions (individual or combinations thereof) could be occurring, and a much more in-depth study is needed to unambiguously determine the identity of these. But we can surmise that these interactions would first result from the formation of metal−organic oligomers of titanium methoxide and titanium isopropoxide.[38] Additionally, there could be exchange of alkoxide ligands with the carboxylate ligands of BDC forming MOF precursors.[39] Finally, the surfactant molecules could cap the MOF precursors. This interaction has been seen in both zeolite and MOF syntheses in which surfactants have been used to cap crystals and modulate crystal growth.[27−34] Furthermore, DBT oxidation was attempted with a meso-MIL-125 catalyst prior to surfactant removal. No catalysis occurred indicating that the external active sites were blocked by the CTAB capping the MOF particles. Afterward, the solvent (MeOH) is removed under vacuum, embedding the prepolymerized metal−organic oligomers in place in an organic/inorganic matrix composed of the surfactant. This process has been suggested by both Naik et al.[27,28] and Sakthivel et al.[29] during synthesis of zeolites by surfactant modulated dry gel conversion methods. This embedding process is crucial to the synthesis because it immobilizes the MOF precursors in a confined environment during VAC, preventing the formation of large crystals and allowing for the production of mesoporous aggregates of small particles. This was corroborated by an additional synthetic experiment in which MOF precursors were directly mixed and subjected to VAC without an embedding stage (e.g., methanol mixing and removal). The resulting MOF displayed inferior pore properties and no interparticle mesoporosity. When the precursor-embedded matrix is correctly formed and subjected to VAC, the solvent (DMF/MeOH) is vaporized and condensed on the solid precursor powder allowing for solvent/precursor interaction. Due to the high concentration of well-mixed reactants, the MOF precursors undergo fast crystallization as seen in zeolite synthesis by similar methods.[40,41] This physical phenomenon is also crucial to the synthesis of the mesoporous MOF because dissolution of the embedded matrix in a solvent during a solvothermal process resulted in a microporous MOF but failed to yield interparticle mesoporosity, which indicated the need to retain the confined environment present in a VAC synthesis. As an additional check, we also synthesized MIL-125 solvothermally with the addition of CTAB and citric acid as a cooperative template following reported methods. Again, the resulting MOF was not mesoporous, which further highlighted the need for the VAC method when synthesizing mesoporous MIL-125.

To demonstrate the benefits of mesoporosity, we tested the optimum meso-MIL-125 material along with both solv-micro-MIL-125 and VAC-micro-MIL-125 for catalytic activity in the oxidation of DBT by *tert*-butyl hydroperoxide and the results



DOI: 10.1021/am508799d
*ACS Appl. Mater. Interfaces* 2015, 7, 5338−5346

are shown in Figure 6 and summarized in Table 1. It should be noted here that DBT is initially oxidized to its corresponding

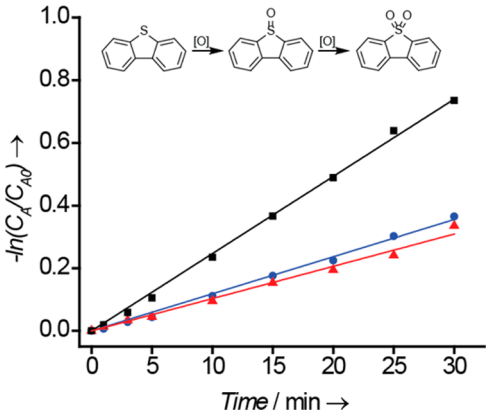


**Figure 6.** Fitting of experimental data to a pseudo-first-order rate model in the oxidation of DBT for (blue ●) solv-micro-MIL-125, (red ▲) VAC-micro-MIL-125, and (black ■) meso-MIL-125. Reaction conditions: 88 $\mu$mol Ti metal centers, 21.9 g of decane, 0.5 g of dodecane, 0.065 g of DBT (500 ppmw sulfur), TBHP in a 10:1 TBHP:DBT molar ratio, 80 °C reaction temperature.

sulfoxide and subsequently oxidized to the corresponding sulfone through a series reaction. In this work, only the sulfone was detected via both GC-FID and GC-MS. Apparent reaction rate constants were determined by fitting experimental data to a pseudo-first-order model. As noted previously and shown in Figure 6, DBT is a heterocyclic, aromatic, sulfur containing compound that is too bulky to fit into the micropores of MIL-125.[9] Thus, the addition of interparticle mesoporosity in the MIL-125 structure large enough to accommodate DBT should have a significant effect on catalysis by allowing access to more active sites. The solv-micro-MIL-125 sample exhibited a similar rate constant ($k_{app}$ = 11.8 × $10^{-3}$ $min^{-1}$) to its microporous VAC analogue ($k_{app}$ = 11.6 × $10^{-3}$ $min^{-1}$), which was attributed to the similar surface areas of the two samples. The meso-MIL-125 sample, however, displayed significantly increased activity ($k_{app}$ = 22.9 × $10^{-3}$ $min^{-1}$) despite having a lower total surface area than both microporous samples. Furthermore, the meso-MIL-125 material retained its high activity and crystalline MOF structure upon subsequent recycle reactions (Figures S11 and S12, Supporting Information). These recycle results indicated the VAC method of synthesis with CTAB provided a reproducible catalytic activity enhancement compared to the microporous MOF.

It is widely believed that catalytic oxidation of DBT using Ti materials proceeds through unsaturated Ti metal centers.[42,43] Therefore, the enhancement in catalytic activity exhibited by meso-MIL-125 could be attributed to two sources: (1) the addition of mesopores, which exposed a relatively higher amount of unsaturated metal sites that were accessible to the bulky DBT molecule but were unavailable or inaccessible in the microporous analogues or (2) the presence of newly formed and alternative active Ti surface sites. If the surface of each material (microporous or mesoporous) is truly comprised of the same type of unsaturated Ti species as catalytically active sites, the initial reaction rates normalized on accessible catalytic surface area, which includes external and interparticle mesoporous surface areas, should be equal for all materials. As expected, the normalized initial reaction rates for all materials were nearly identical (Table 1, ~22.0 × $10^{-7}$ $mol_{DBT}$ $min^{-1}$ $m^2_{accessible}$) indicating the VAC method for introducing mesoporosity did not alter the nature of the catalytic sites but instead provided enhanced accessibility to active sites.

To further investigate this claim, we performed adsorption studies and used this data to calculate heats of adsorption for all materials. The heat of adsorption is an indicator of the strength of interaction between an adsorbate and an adsorbent and could be used to glean insight about the energetics of a catalytic mechanism. Moreover, multiple studies have shown that organosulfur compounds can adsorb to coordinatively unsaturated metal sites in MOFs.[44,45] Thiophene is an organosulfur compound that is similar in structure to DBT except it does not contain the two fused phenyl side rings. Rather, it is a five-membered heterocyclic aromatic sulfur compound with a kinetic diameter of 4.6 Å, which allows it to fit into the micropores of MIL-125.[46] The heats of adsorption of thiophene on the MIL-125 samples were determined via a TGA/DSC experiment (see the Experimental Section for details). In this experiment, $N_2$ was bubbled through thiophene (bp = 84 °C) and over the samples which were kept isothermal at 90 °C, while heat flow and weight were monitored as a function of adsorption time. The heats of adsorption of thiophene on the MIL-125 samples as a function of coverage is shown in Figure 7. All three samples showed similar heats of adsorption

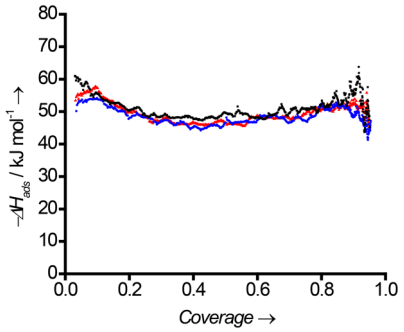


**Figure 7.** Heats of adsorption of thiophene for (blue ●) solv-micro-MIL-125, (red ▲) VAC-micro-MIL-125, and (black ■) meso-MIL-125. For clarity, fluctuations in data at low coverage (<0.03) and high coverage (>0.95) were excluded in the plot.

(average $\Delta H_{ads}$ = −48.5 ± 1.4 kJ $mol^{-1}$) for coverages between 0.1 and 0.8. While these results cannot be used to identify the different types of active sites present, they can, however, be used to suggest that the active sites in the MIL-125 samples were all energetically equivalent.[47] This adsorption study further corroborates the claim that the meso-MIL-125 does not contain a new type of active site, but rather the addition of interparticle mesoporosity was responsible for the increase in activity seen in the DBT oxidation reaction due to enhanced accessibility. Of additional note, the meso-MIL-125 sample also had a larger capacity for thiophene adsorption (0.65 $mol_{thiophene}$ $mol_{Ti}^{-1}$) than the microporous solvothermal and VAC samples (0.53 and 0.55 $mol_{thiophene}$ $mol_{Ti}^{-1}$, respectively). Because the microporous samples have higher total surface areas than the mesoporous sample, these results suggest that the mesoporous sample actually contained a higher density of active sites than the microporous materials. These additional active sites are likely located on both the external surface and inside the interparticle mesopores where the unit cells of the MIL-125


DOI: 10.1021/am508799d
ACS Appl. Mater. Interfaces 2015, 7, 5338−5346

crystals are truncated leading to the formation of unsaturated metal centers.

## 4. CONCLUSION

In summary, the first example of MIL-125 synthesized using a vapor-assisted crystallization method was demonstrated. The VAC-synthesized MIL-125 showed similar properties to a solvothermally synthesized analogue. The VAC method could then be adapted to add interparticle mesoporosity to MIL-125 through the use of a surfactant (CTAB). The surfactant likely acted as a capping agent creating confined local environments of MOF precursors, which then crystallized and formed mesoporous aggregates of nanosized MOF particles. This synthetic method marked a significant achievement because it allowed for the synthesis of hierarchical microporous/mesoporous MIL-125 without the use of a chelating agent. Moreover, the importance of the VAC method was emphasized because the addition of mesoporosity could not be easily accomplished using typical solvothermal methods. Catalytic tests in the oxidation of an aromatic sulfur compound (DBT) demonstrated the hierarchical MIL-125 displayed a marked enhancement in activity over its microporous analogues. Normalization of initial reaction rates on accessible surface area in conjunction with thiophene studies indicated that the enhancement in catalytic activity was due to the addition of mesoporosity rather than the formation of different active sites. Furthermore, thiophene adsorption studies suggested that the surfactant modified VAC method could lead to exposure of additional active sites resulting in higher measured catalytic activities.

## ■ ASSOCIATED CONTENT

### Supporting Information

Schematic of precursor gel preparation, powder XRD patterns for microporous MIL-125 synthesized via VAC, $N_2$ physisorption isotherms of microporous MIL-125, powder XRD pattern of mesoporous MIL-125, TEM of mesoporous MIL-125, TGA data for microporous and mesoporous MIL-125, UV−vis spectrum of mesoporous MIL-125, textural properties of MIL-125 synthesized solvothermally with CTAB, pore size distribution of solvothermally synthesized MIL-125 with CTAB, catalytic recycle studies for mesoporous MIL-125, XRD pattern of mesoporous MIL-125 after recycle. This material is available free of charge via the Internet at http://pubs.acs.org.

## ■ AUTHOR INFORMATION

### Corresponding Author

*E-mail: jhicks3@nd.edu.

### Notes

The authors declare no competing financial interest.

## ■ ACKNOWLEDGMENTS

Acknowledgement is made to the Donors of the American Chemical Society Petroleum Research Fund for support of this research (PRF# 53874-DNI10). This work was completed with the use of the Center for Sustainable Energy at Notre Dame's Bruker D8 Advanced Davinci diffractometer and Micrometrics ASAP-2020 Physisorption Analyzer. TEM and SEM images were acquired using the Notre Dame Integrated Imaging Facility's FEI Titan microscope and FEI-Magellan FESEM, respectively. We thank the Center for Environmental Science and Technology for use of the center's Optima 8000 ICP-OES.

## ■ REFERENCES

(1) Chen, X.; Mao, S. S. Titanium Dioxide Nanomaterials: Synthesis, Properties, Modifications, and Applications. *Chem. Rev.* **2007**, *107*, 2891−2959.

(2) Trukhan, N. N.; Romannikov, V. N.; Shmakov, A. N.; Vanina, M. P.; Paukshtis, E. A.; Bukhtiyarov, V. I.; Kriventsov, V. V.; Danilov, I. Y.; Kholdeeva, O. A. $H_2O_2$-Based Selective Oxidations Over Titaniumsilicates of SBA-15 Type. *Microporous Mesoporous Mater.* **2003**, *59*, 73−84.

(3) Dan-Hardi, M.; Serre, C.; Frot, T.; Rozes, L.; Maurin, G.; Sanchez, C.; Ferey, G. A New Photoactive Crystalline Highly Porous Titanium(IV) Dicarboxylate. *J. Am. Chem. Soc.* **2009**, *131*, 10857−10859.

(4) Fu, Y.; Sun, D.; Chen, Y.; Huang, R.; Ding, Z.; Fu, X.; Li, Z. An Amine-Functionalized Titanium Metal-Organic Framework Photocatalyst with Visible-Light-Induced Activity for $CO_2$ reduction. *Angew. Chem., Int. Ed. Engl.* **2012**, *51*, 3364−3367.

(5) Toyao, T.; Saito, M.; Horiuchi, Y.; Mochizuki, K.; Iwata, M.; Higashimura, H.; Matsuoka, M. Efficient Hydrogen Production and Photocatalytic Reduction of Nitrobenzene Over a Visible-Light-Responsive Metal−Organic Framework Photocatalyst. *Catal. Sci. Technol.* **2013**, *3*, 2092−2097.

(6) Horiuchi, Y.; Toyao, T.; Saito, M.; Mochizuki, K.; Iwata, M.; Higashimura, H.; Anpo, M.; Matsuoka, M. Visible-Light-Promoted Photocatalytic Hydrogen Production by Using an Amino-Functionalized Ti(IV) Metal−Organic Framework. *J. Phys. Chem. C* **2012**, *116*, 20848−20853.

(7) Ivanchikova, I. D.; Lee, J. S.; Maksimchuk, N. V.; Shmakov, A. N.; Chesalov, Y. A.; Ayupov, A. B.; Hwang, Y. K.; Jun, C.-H.; Chang, J.-S.; Kholdeeva, O. A. Highly Selective $H_2O_2$-Based Oxidation of Alkylphenols to $\rho$-Benzoquinones Over MIL-125 Metal−Organic Frameworks. *Eur. J. Inorg. Chem.* **2014**, *2014*, 132−139.

(8) Kim, S.-N.; Kim, J.; Kim, H.-Y.; Cho, H.-Y.; Ahn, W.-S. Adsorption/Catalytic Properties of MIL-125 and $NH_2$-MIL-125. *Catal. Today* **2013**, *204*, 85−93.

(9) McNamara, N. D.; Neumann, G. T.; Masko, E. T.; Urban, J. A.; Hicks, J. C. Catalytic Performance and Stability of (V) MIL-47 and (Ti) MIL-125 in the Oxidative Desulfurization of Heterocyclic Aromatic Sulfur Compounds. *J. Catal.* **2013**, *305*, 217−226.

(10) Lee, J.; Farha, O. K.; Roberts, J.; Scheidt, K. A.; Nguyen, S. T.; Hupp, J. T. Metal−Organic Framework Materials as Catalysts. *Chem. Soc. Rev.* **2009**, *38*, 1450−1459.

(11) Kim, J.; McNamara, N. D.; Her, T. H.; Hicks, J. C. Carbothermal Reduction of Ti-modified IRMOF-3: An Adaptable Synthetic Method to Support Catalytic Nanoparticles on Carbon. *ACS Appl. Mater. Interfaces* **2013**, *5*, 11479−11487.

(12) Eddaoudi, M.; Kim, J.; Rosi, N.; Vodak, D.; Wachter, J.; O'Keeffe, M.; Yaghi, O. M. Systematic Design of Pore Size and Functionality in Isoreticular MOFs and Their Application in Methane Storage. *Science* **2002**, *295*, 469−472.

(13) Liu, Y. Y.; Couck, S.; Vandichel, M.; Grzywa, M.; Leus, K.; Biswas, S.; Volkmer, D.; Gascon, J.; Kapteijn, F.; Denayer, J. F.; Waroquier, M.; Van Speybroeck, V.; Van Der Voort, P. New V(IV)-Based Metal−Organic Framework Having Framework Flexibility and High $CO_2$ Adsorption Capacity. *Inorg. Chem.* **2013**, *52*, 113−120.

(14) Deng, H.; Grunder, S.; Cordova, K. E.; Valente, C.; Furukawa, H.; Hmadeh, M.; Gandara, F.; Whalley, A. C.; Liu, Z.; Asahina, S.; Kazumori, H.; O'Keeffe, M.; Terasaki, O.; Stoddart, J. F.; Yaghi, O. M. Large-Pore Apertures in a Series of Metal−Organic Frameworks. *Science* **2012**, *336*, 1018−1023.

(15) Schnobrich, J. K.; Koh, K.; Sura, K. N.; Matzger, A. J. A Framework for Predicting Surface Areas in Microporous Coordination Polymers. *Langmuir* **2010**, *26*, 5808−5814.

(16) Qiu, L. G.; Xu, T.; Li, Z. Q.; Wang, W.; Wu, Y.; Jiang, X.; Tian, X. Y.; Zhang, L. D. Hierarchically Micro- and Mesoporous Metal-



DOI: 10.1021/am508799d
*ACS Appl. Mater. Interfaces* 2015, 7, 5338−5346

Organic Frameworks with Tunable Porosity. *Angew. Chem., Int. Ed. Engl.* **2008**, *47*, 9487−9491.
(17) Zhao, Y.; Zhang, J.; Han, B.; Song, J.; Li, J.; Wang, Q. Metal-Organic Framework Nanospheres with Well-Ordered Mesopores Synthesized in an Ionic Liquid/$CO_2$/Surfactant System. *Angew. Chem., Int. Ed. Engl.* **2011**, *50*, 636−639.
(18) Pham, M.-H.; Vuong, G.-T.; Fontaine, F.-G.; Do, T.-O. A Route to Bimodal Micro-Mesoporous Metal−Organic Frameworks Nanocrystals. *Cryst. Growth Des.* **2012**, *12*, 1008−1013.
(19) Sun, L. B.; Li, J. R.; Park, J.; Zhou, H. C. Cooperative Template-Directed Assembly of Mesoporous Metal−Organic Frameworks. *J. Am. Chem. Soc.* **2012**, *134*, 126−129.
(20) Bradshaw, D.; El-Hankari, S.; Lupica-Spagnolo, L. Supramolecular Templating of Hierarchically Porous Metal−Organic Frameworks. *Chem. Soc. Rev.* **2014**, *43*, 5431−5443.
(21) Furukawa, S.; Reboul, J.; Diring, S.; Sumida, K.; Kitagawa, S. Structuring of Metal-Organic Frameworks at the Mesoscopic/Macroscopic Scale. *Chem. Soc. Rev.* **2014**, *43*, 5700−5734.
(22) Abedi, S.; Morsali, A. Ordered Mesoporous Metal−Organic Frameworks Incorporated with Amorphous $TiO_2$ As Photocatalyst for Selective Aerobic Oxidation in Sunlight Irradiation. *ACS Catal.* **2014**, *4*, 1398−1403.
(23) Yue, Y.; Qiao, Z. A.; Fulvio, P. F.; Binder, A. J.; Tian, C.; Chen, J.; Nelson, K. M.; Zhu, X.; Dai, S. Template-Free Synthesis of Hierarchical Porous Metal−Organic Frameworks. *J. Am. Chem. Soc.* **2013**, *135*, 9572−9575.
(24) Xuan, W.; Zhu, C.; Liu, Y.; Cui, Y. Mesoporous Metal-Organic Framework Materials. *Chem. Soc. Rev.* **2012**, *41*, 1677−1695.
(25) Cao, S.; Gody, G.; Zhao, W.; Perrier, S.; Peng, X.; Ducati, C.; Zhao, D.; Cheetham, A. K. Hierarchical Bicontinuous Porosity in Metal−Organic Frameworks Templated from Functional Block Co-oligomer Micelles. *Chem. Sci.* **2013**, *4*, 3573−3577.
(26) Wee, L. H.; Wiktor, C.; Turner, S.; Vanderlinden, W.; Janssens, N.; Bajpe, S. R.; Houthoofd, K.; Van Tendeloo, G.; De Feyter, S.; Kirschhock, C. E.; Martens, J. A. Copper Benzene Tricarboxylate Metal−Organic Framework with Wide Permanent Mesopores Stabilized by Keggin Polyoxometallate Ions. *J. Am. Chem. Soc.* **2012**, *134*, 10911−10919.
(27) Naik, S. P.; Chen, J. C.; Chiang, A. S. T. Synthesis of Silicalite Nanocrystals via the Steaming of Surfactant Protected Precursors. *Microporous Mesoporous Mater.* **2002**, *54*, 293−303.
(28) Naik, S. P.; Chiang, A. S. T.; Thompson, R. W. Synthesis of Zeolitic Mesoporous Materials by Dry Gel Conversion under Controlled Humidity. *J. Phys. Chem. B* **2003**, *107*, 7006−7014.
(29) Sakthivel, A.; Iida, A.; Komura, K.; Sugi, Y.; Chary, K. V. R. Nanosized $\beta$-zeolites with Tunable Particle Sizes: Synthesis by the Dry Gel Conversion (DGC) Method in the Presence of Surfactants, Characterization and Catalytic Properties. *Microporous Mesoporous Mater.* **2009**, *119*, 322−330.
(30) Taylor, K. M.; Jin, A.; Lin, W. Surfactant-Assisted Synthesis of Nanoscale Gadolinium Metal−Organic Frameworks for Potential Multimodal Imaging. *Angew. Chem., Int. Ed. Engl.* **2008**, *47*, 7722−7725.
(31) Ma, M.; Zacher, D.; Zhang, X.; Fischer, R. A.; Metzler-Nolte, N. A Method for the Preparation of Highly Porous, Nanosized Crystals of Isoreticular Metal−Organic Frameworks. *Cryst. Growth Des.* **2011**, *11*, 185−189.
(32) Pan, Y.; Heryadi, D.; Zhou, F.; Zhao, L.; Lestari, G.; Su, H.; Lai, Z. Tuning the Crystal Morphology and Size of Zeolitic Imidazolate Framework-8 in Aqueous Solution by Surfactants. *CrystEngComm* **2011**, *13*, 6937−6940.
(33) Peng, L.; Zhang, J.; Li, J.; Han, B.; Xue, Z.; Yang, G. Surfactant-Directed Assembly of Mesoporous Metal−Organic Framework Nanoplates in Ionic Liquids. *Chem. Commun.* **2012**, *48*, 8688−8690.
(34) Sarawade, P.; Tan, H.; Polshettiwar, V. Shape- and Morphology-Controlled Sustainable Synthesis of Cu, Co, and In Metal Organic Frameworks with High $CO_2$ Capture Capacity. *ACS Sustainable Chem. Eng.* **2012**, *1*, 66−74.
(35) Ahmed, I.; Jeon, J.; Khan, N. A.; Jhung, S. H. Synthesis of a Metal−Organic Framework, Iron-Benezenetricarboxylate, from Dry Gels in the Absence of Acid and Salt. *Cryst. Growth Des.* **2012**, *12*, 5878−5881.
(36) Shi, Q.; Chen, Z.; Song, Z.; Li, J.; Dong, J. Synthesis of ZIF-8 and ZIF-67 by Steam-Assisted Conversion and an Investigation of Their Tribological Behaviors. *Angew. Chem., Int. Ed. Engl.* **2011**, *50*, 672−675.
(37) Sang, L.; Zhao, Y.; Burda, C. $TiO_2$ Nanoparticles as Functional Building Blocks. *Chem. Rev.* **2014**, *114*, 9283−9318.
(38) Wright, D. A.; Williams, D. A. The Crystal and Molecular Structure of Titanium Tetramethoxide. *Acta Crystallogr.* **1968**, *B24*, 1107−1114.
(39) Boyle, T. J.; Tyner, R. P.; Alam, T. M.; Scott, B. L.; Ziller, J. W.; Potter, B. G., Jr. Implications for the Thin-Film Densification of $TiO_2$ from Carboxylic Acid-Modified Titanium Alkoxides. Syntheses, Characterizations, X-ray Structures of $Ti_3(\mu_3\text{-}O)(O_2CH)_2(ONep)_8$, $Ti_3(\mu_3\text{-}O)(O_2CMe)_2(ONep)_8$, $Ti_6(\mu_3\text{-}O)_6(O_2CCHMe_2)_6(ONep)_6$, $[Ti(\mu\text{-}O_2CCMe_3)(ONep)_3]_2$, and $Ti_3(\mu_3\text{-}O)(O_2CCH_2CMe_3)_2(ONep)_8$ (ONep = $OCH_2CMe_3$). *J. Am. Chem. Soc.* **1999**, *121*, 12104−12112.
(40) Matsukata, M.; Ogura, M.; Osaki, T.; Hari Prasad Rao, P. R.; Nomura, M.; Kikuchi, E. Conversion of Dry Gel to Microporous Crystals in Gas Phase. *Top. Catal.* **1999**, *9*, 77−92.
(41) Neumann, G. T.; Hicks, J. C. Dual Roles of Steam in the Dry Gel Synthesis of Mesoporous ZSM-5. *Cryst. Growth Des.* **2013**, *13*, 1535−1542.
(42) Liu, Z.; Crumbaugh, G. M.; Davis, R. J. Effect of Structure and Composition on Epoxidation of Hexene Catalyzed by Microporous and Mesoporous Ti-Si Mixed Oxides. *J. Catal.* **1996**, *159*, 83−89.
(43) Kim, T.-W.; Kim, M.-J.; Kleitz, F.; Nair, M. M.; Guillet-Nicolas, R.; Jeong, K.-E.; Chae, H.-J.; Kim, C.-U.; Jeong, S.-Y. Tailor-Made Mesoporous Ti-SBA-15 Catalysts for Oxidative Desulfurization of Refractory Aromatic Sulfur Compounds in Transport Fuel. *ChemCatChem.* **2012**, *4*, 687−697.
(44) Peralta, D.; Chaplais, G.; Simon-Masseron, A.; Barthelet, K.; Pirngruber, G. D. Metal−Organic Framework Materials for Desulfurization by Adsorption. *Energy Fuels* **2012**, *26*, 4953−4960.
(45) Wu, L.; Xiao, J.; Wu, Y.; Xian, S.; Miao, G.; Wang, H.; Li, Z. A Combined Experimental/Computational Study on the Adsorption of Organosulfur Compounds Over Metal−Organic Frameworks From Fuels. *Langmuir* **2014**, *30*, 1080−1088.
(46) Zeng, Y.; Ju, S. Adsorption of Thiophene and Benzene in Sodium-Exchanged MFI- and MOR-Type Zeolites: A Molecular Simulation Study. *Sep. Purif. Technol.* **2009**, *67*, 71−78.
(47) Parrillo, D. J.; Lee, C.; Gorte, R. J. Heats of Adsorption for Ammonia and Pyridine in H-ZSM-5: Evidence for Identical Brønsted-Acid Sites. *Appl. Catal., A* **1994**, *110*, 67−74.


DOI: 10.1021/am508799d
*ACS Appl. Mater. Interfaces* 2015, 7, 5338−5346